# A constrained least-squares approach to the automated quantitation of *in-vivo* $^1$H MRS data.

Martin Wilson[1,2*], Greg Reynolds[3*], Risto A. Kauppinen[4], Theodoros N. Arvanitis[5,2] and Andrew C. Peet[1,2]

[1] Cancer Sciences, University of Birmingham, Birmingham, United Kingdom.

[2] Birmingham Children's Hospital NHS Foundation Trust, Birmingham, United Kingdom.

[3] Pattern Analytics Ltd, Birmingham, United Kingdom.

[4] Department of Radiology, Dartmouth College, Hanover, NH, United States.

[5] School of Electronic, Electrical and Computer Engineering, University of Birmingham, Birmingham, United Kingdom.

[*] Contributed equally as first authors to this work.

**Correspondence to:** Martin Wilson, Academic Department of Paediatrics and Child Health, Birmingham Children's Hospital, Steelhouse Lane, Birmingham, West Midlands, B4 6NH, UK, Tel No.: 01213338744, Email to: martin@pipegrep.co.uk.

**Running title:** Automated quantitation of *in-vivo* $^1$H MRS data.

**Word count:** 6457

**Abstract**

TARQUIN, a new method for the fully automatic analysis of short echo-time *in-vivo* $^{1}$H MRS is presented. Analysis is performed in the time-domain using non-negative least-squares and a new method for applying soft constraints to signal amplitudes is employed to improve fitting stability. Initial point truncation and HSVD water removal are used to reduce baseline interference. Three methods were used to test performance. Firstly, metabolite concentrations from six healthy volunteers at 3T were compared with LCModel$^{TM}$. Secondly, a Monte-Carlo simulation was performed and results were compared with LCModel$^{TM}$ to test the accuracy of the new method. Finally, the new algorithm was applied to 1956 spectra, acquired clinically at 1.5T, to test robustness to noisy, abnormal, artefactual and poorly shimmed spectra. Discrepancies of less than approximately 20% were found between the main metabolite concentrations determined by TARQUIN and LCModel$^{TM}$ from healthy volunteer data. The Monte-Carlo simulation revealed that errors in metabolite concentration estimates were comparable to LCModel$^{TM}$. TARQUIN analyses were also found to be robust to clinical data of variable quality. In conclusion, TARQUIN has been shown to be an accurate and robust algorithm for the analysis of MRS data making it suitable for use in a clinical setting.

**Key words:** magnetic resonance spectroscopy (MRS), quantitation, brain, tumour.

# 1 Introduction

Many algorithms have been proposed to solve the problem of quantifying signals present in $^{1}$H *in-vivo* MRS data (1). The most popular methods can be categorised as follows: black box, peak fitting and basis-set. Black-box methods are usually based on either the LPSVD (2) or HSVD (3) methods, which can be made computationally efficient (HLSVD (4)) for *in-vivo* data, and are effective at extracting peak parameters from simple spectra. One drawback of black-box methods is that additional knowledge of spectral features cannot be incorporated into the algorithm allowing infeasible results to be possible for more complex data. For example, an incorrect ratio between peaks originating from the same molecule is possible. The AMARES (5) algorithm was developed to address this issue by extending the VARPRO (6) peak fitting method to allow a greater level of prior knowledge to be incorporated into the fitting model.

Black-box and peak fitting methods have been shown to be highly effective for sparse spectra such as long-echo $^{1}$H or $^{31}$P MRS, however the complex patterns of some metabolites seen in short echo $^{1}$H MRS data are cumbersome to model as a series of single peaks. Whilst long echo-time $^{1}$H MRS is still popular, there is a growing trend to shorter echo times (7) due to the increase in metabolic information. Therefore, analysis methods which are suited to this data type are becoming increasingly important. For complex data, methods that incorporate a metabolite basis set have been shown to be more effective than peak fitting methods (8).

LCModel$^{\text{TM}}$(9) was one of the first algorithms to incorporate a metabolite basis set into the fitting model and is widely used for the analysis of short-echo time $^{1}$H MRS data. The algorithm models data in the frequency domain using a linear combination of metabolite, lipid and macromolecule signals combined with a smoothing splines to account for baseline signals. More recently the QUEST (10) algorithm has been developed that uses a combination of time-domain fitting and HSVD to model background signals. An alternative approach is taken by AQSES (11) that uses a combination of time-domain fitting and penalized splines to model the baseline. AQSES also differs from LCModel$^{\text{TM}}$ and QUEST as it employs the variable projection method to estimate the amplitudes of the metabolite basis set resulting in a reduction in the number of model parameters. This method of amplitude estimation is also used by the TARQUIN method for analysis of high resolution NMR spectra (12) and the ProFit method (13), which is optimised for fitting J-resolved spectra.

In this paper a variant of our previously published work, TARQUIN (Totally Automatic Robust Quantitation in NMR) (12), is presented that uses time-domain truncation to eliminate baseline interference and models the remaining signal with a parametrised basis set containing metabolites,

lipids and macromolecules in the time-domain. Like the AQSES algorithm, a non-negative least-squares projection is used to estimate signal amplitudes. In contrast to QUEST and AQSES, lipids and macromolecule signals are included in the basis set and a new method is presented for imposing soft constraints on the least-squares projection to reduce errors associated with overfitting. To validate the method, short echo MRS data taken from the parietal white matter of six healthy volunteers will be analysed and compared with LCModel$^{\mathrm{TM}}$ and published values. A Monte-Carlo simulation will be performed to asses the accuracy of the method compared to LCModel$^{\mathrm{TM}}$. Robustness is an important property of any fitting method used for clinical applications. We define robustness as the successful automated analysis of data typically acquired clinically, which includes: noisy, abnormal, artefactual and poorly shimmed spectra. To test the robustness of TARQUIN, a large series of clinically acquired spectra will be analysed and their fit quality assessed.

# 2 Method

## 2.1 Algorithmic Details

The algorithm consists of three main parts: preprocessing, basis set simulation and the solution of a non-linear least squares fitting problem, each of which is described in the following section.

Throughout the rest of the paper the following conventions are adopted: vector and matrix quantities are denoted in bold, scalars are not. The $N$ point time domain signal being analysed is $\boldsymbol{y} \in \mathbb{C}^N$, its complex Fourier transform is $\boldsymbol{Y} \in \mathbb{C}^N$. The sampling frequency is denoted $f_s$, the zero and first order phase correction terms are written $\phi_0$ and $\phi_1$. It is often convenient to refer to only a subset of the samples in the FID, the start of this range is denoted $n_s$ and the end $n_e$. We denoted the water reference signal as $\boldsymbol{y}_W$.

### 2.1.1 Water Removal by HSVD

Post acquisition residual water is removed by modelling the signal within a user specified frequency range, where the full spectral width ranges from $-\frac{f_s}{2}$ to $+\frac{f_s}{2}$Hz. Since the default basis set only contains signals upfield from the water resonance and the residual water peak was found to occupy frequencies up to around 45Hz, a range of $[-\frac{f_s}{2}, +45]$Hz is modelled for removal as it rarely contains useful data. The model is constructed using the HSVD method (3) and subsequently subtracted from the FID. Computationally efficient implementations of this method are discussed in (14), which also reviews the HSVD technique.

### 2.1.2 Automatic Phasing

The TARQUIN algorithm accounts for phase adjustments in two ways. During the preprocessing stage, a zero-order phase correction term is found, as mentioned below, which is applied to the signal undergoing analysis. This initial phasing step makes visual inspection of the spectra easier and is useful in assessing the quality of the other preprocessing steps. During the fitting stage, zero and first order correction terms $\Delta\phi_0$ and $\Delta\phi_1$ are computed and applied to the basis set. The initial estimate for $\phi_0$ is obtained by minimising the difference between the magnitude and real spectra, i.e. we solve the following optimisation problem:

$$\phi_0 = \arg\min_{\hat{\phi}_0} \sum_{n=0}^{N-1} \left[ |\boldsymbol{Y}[n]| - \mathsf{Re}\left\{ \boldsymbol{Y}[n] \exp(j\hat{\phi}_0) \right\} \right]^2 \tag{1}$$

### 2.1.3 Automatic Referencing

For *in-vivo* $^1$H MRS it is standard for the reference frequency to be adjusted, such that the water signal resonates at the exact centre of the spectrum at 0Hz. However, imperfections in the static field often cause a minor frequency shift that can hamper quantitation.

For an NMR spectrum, the chemical shift scale vector: `ppm`, is defined as follows:

$$\texttt{ppm}[n] = \texttt{ref} + \frac{10^6}{f_R}\left(-\frac{f_s}{2} + \frac{f_s}{N}n\right) \tag{2}$$

where $f_R$ is the static magnetic field strength measured in Hz and `ref` represents the chemical shift value at the centre of the spectrum (typically 4.7ppm for $^1$H MRS). The value of `ref` needs to be determined for each spectrum for fitting to be optimal. The method chosen involves finding the cross-correlation between the absolute value of the acquired spectrum $|\boldsymbol{Y}|$ and a reference spectrum $|\boldsymbol{R}|$. The reference spectrum is composed of several synthesised narrow peaks that are typically present in the tissue under investigation. For brain tissue, peaks at 2.01, 3.22 and 3.03ppm, are suitable for aligning the spectrum to NAA, total-choline and creatine respectively. For tumour data, it can be helpful to add peaks at 1.28 and 0.9ppm to allow lipids to be used as reference points in the absence of metabolite signals. Once the cross-correlation function is found, the maximum will correspond to the best match between the two signals and the correct value of `ref` can be calculated. Finally the basis-set and chemical shift scale vector are updated to account for this offset.

As part of the algorithm, the acquired spectrum is first zero-filled to twice its original length to obtain `ref` at a higher precision, and the cross-correlation is calculated efficiently using the fast Fourier transform method, widely used in signal processing. A by-product of this process is

that an approximation to the common spectral linewidth can also be determined by measuring the full width at half maximum (FWHM) of the cross-correlation function. This approximate value is used to determine an initial value for the common damping term $\beta$, defined in a subsequent section describing the signal model.

### 2.1.4 Basis Set Simulation

Basis sets are simulated using an in-house implementation of the density matrix formulation of NMR, a comprehensive description of the theoretical background and computational methods are provided by Levitt (15) and Smith et al. (16) respectively. The PRESS sequence was simulated using ideal pulses with $t_1 = 6.3$ms whilst $t_2$ was automatically adjusted to match the exact echo time of sequence (see (17) for details of the PRESS pulse sequence). $T_1$ and $T_2$ relaxation, during the evolution periods, were not modelled in the simulation.

Chemical shift and J-coupling values from Govinderaju et al. (18) were used to simulate the following metabolites: alanine (Ala), aspartate (Asp), creatine (Cr), gamma-aminobutyric acid (GABA), glucose (Glc), glutamine (Gln), glutamate (Glu), guanidinoacetate (Gua), myo-inositol (m-Ins), lactate (Lac), N-acetyl-aspartate (NAA), N-acetyl-aspartylglutamate (NAAG), scyllo-inositol (s-Ins), taurine (Tau), glycerophosphorylcholine (GPC) and phosphorylcholine (PC). Each metabolite was simulated with a Lorenzian lineshape with a FWHM of 0.8Hz. The accuracy of this basis set compared with experimentally derived metabolite spectra has previously been demonstrated (19).

In addition to metabolites, lipid and macromolecular components were added to the basis set. To allow a direct comparison with LCModel$^{\text{TM}}$, the same default lipid and macromolecular components were used. Details of the parameters used to simulate the signals are provided in Table 1.

### 2.1.5 Signal Model

TARQUIN uses the approach of modelling the experimental data as a linear combination of modified simulated basis signals. The modifications are required to account for minor differences in the lineshape and frequency of the basis signals, accounting for small changes in the relaxation, shimming and chemical environment of the resonant molecules. The complete signal model $\hat{\boldsymbol{y}}$ is described by the following equation:

$$\hat{\boldsymbol{y}}[n] = \sum_{i=1}^{M} a_i \left[\texttt{phase}(\boldsymbol{s}_i, \Delta\phi_0, \Delta\phi_1)[n] \exp\left(\left[j\Delta\omega_i - \Delta\alpha_i - \beta n\Delta t\right] n\Delta t\right)\right] \tag{3}$$

$\hat{\boldsymbol{y}}$ represents the sum of each basis vector $\boldsymbol{s}_i$ weighted by its amplitude $a_i$. The $\Delta\omega_i$ and $\Delta\alpha_i$ terms represent the frequency shift and Lorentzian damping adjustment to the $i$-th basis vector respectively. The $\beta$ term is the common Gaussian damping, shared across all signals, which in conjunction with the Lorenztian damping term results in Voigt lineshapes (20) in the frequency domain. The Gaussian damping parameter was included to model imperfect shimming and susceptibility variations that are the same for all signals.. In the model, each basis vector $\boldsymbol{s}_i$ is adjusted by the phase parameters where the `phase`() function is defined as follows. Let $\Upsilon$ denote the discrete Fourier transform of $\boldsymbol{s}$. The phase terms are then applied as:

$$\boldsymbol{\Upsilon}[n] \leftarrow \boldsymbol{\Upsilon}[n] \exp\left(j\Delta\phi_0 + j\Delta\phi_1 2\pi\left(-\frac{f_s}{2} + \frac{f_s}{N}n\right)\right) \tag{4}$$

to obtain the time domain result we take the inverse discrete Fourier transform of $\boldsymbol{\Upsilon}$. $\phi_0$ represents a constant phase shift often present in signals, $\phi_1$ represents a frequency dependent phase shift, which can arise from beginning the acquisition too early or too late. We have chosen to apply the phasing in the frequency domain due to the easier application of the $\phi_1$ parameter. In summary, the complete set of parameters, $\theta$, over which the fitting is performed are:

$$\theta = \{\Delta\omega_i, \Delta\alpha_i : i = 1, \ldots, M\} \cup \{\hat{a}_i : i = 1, \ldots, M\} \cup \{\beta, \Delta\phi_0, \Delta\phi_1\} \tag{5}$$

where $\hat{\boldsymbol{a}}$ is the estimate of true amplitudes $\boldsymbol{a}$. The fitting problem is defined as finding the values of $\theta$ to match the properties of the signal undergoing analysis. However, when the information content of the signal is low and the number of basis set signals is large, overfitting will become a problem. It is therefore desirable to constrain the values of $\theta$ where possible. TARQUIN uses a combination of hard and soft constraints, described in the next section, to improve the stability and accuracy of fitting.

### 2.1.6 Fitting with Constraints

The estimate $\hat{\boldsymbol{y}}(\theta)$ is constructed by minimising the difference between itself and the preprocessed acquired signal, $\boldsymbol{y}$. Mathematically, we find $\theta$ by solving the following problem:

$$\min_{\theta} \sum_{n=n_s}^{n_e} \left(\boldsymbol{y}[n] - \hat{\boldsymbol{y}}(\theta)[n]\right)^2 \tag{6}$$

The difference between the model and the observed signal is only considered over points starting at $n_s$ and ending at $n_e$, where the extremal values for this are 0 and $N-1$ respectively. It is often the case however, that the first few points of the FID contain very broad signals, not easily modelled

with a basis set, and that the last few contain only noise. Visual inspection of the time-domain signals for a number of SVS examinations showed that the vast majority of the signal had decayed by $N/2$ data points. Therefore, a value of $n_e = N/2$ was used to omit the analysis of data points with little or no information content. A value of $n_s = f_s/100$, which corresponded to a truncation of the first 10ms of the FID, was found to be suitable for short echo time $^1$H *in-vivo* MRS data. This value was determined by experimenting with different values across a range of short echo spectra, paying particular attention to the baseline and residual. See Figures 3 and 1 for examples illustrating the effect of $n_s$ on fitting.

A popular approach to the optimisation problem of equation (6) is to use an iterative algorithm, such as Levenberg-Marquardt, to adjust all the parameters to make the model more like the observed data. However, a reduction in the number of parameters that require iterative optimisation can be achieved by determining the linearly entering parameters $\hat{\boldsymbol{a}}$ as a sub-problem at each function evaluation of the iterative optimisation. This approach was chosen for TARQUIN as it has the advantages that starting values are not required for $\hat{\boldsymbol{a}}$, reducing bias, and the complexity of the iterative optimisation problem is reduced. In the following we denote the value of a quantity at a particular iteration of the algorithm, by appending a superscript of the form $(n)$ where $n$ refers to the iteration.

The subproblem of finding $\hat{\boldsymbol{a}}^{(n)}$ can be stated as follows:

$$\min_{\hat{\boldsymbol{a}}^{(n)}} ||\boldsymbol{S}^{(n-1)}\hat{\boldsymbol{a}}^{(n)} - \boldsymbol{y}||_2 \tag{7}$$

where columns of $\boldsymbol{S}^{(n-1)}$ represents the basis signals $\boldsymbol{s}_i$ adjusted by the current set of non-linearly entering parameters. Henceforth, we shall drop the notation for the iteration, and it shall be understood that $\boldsymbol{S}$ refers to $\boldsymbol{S}^{(n-1)}$ for the duration of the amplitude estimation step. Solving for $\hat{\boldsymbol{a}}$ using the pseudo-inverse of $\boldsymbol{S}$ gives:

$$\hat{\boldsymbol{a}} = \boldsymbol{S}^{+}\boldsymbol{y} \tag{8}$$

Solution of the problem in this way has the undesirable property of allowing the elements of $\hat{\boldsymbol{a}}$ to have an arbitrary phase. To constrain the solution to physically meaningful values, we incorporate the prior knowledge that $\hat{\boldsymbol{a}}$ should be non-negative $\hat{\boldsymbol{a}} \geq \boldsymbol{0}$ and have a phase of zero $\hat{\boldsymbol{a}} \in \mathbb{R}^M$. We reform the problem by introducing the new variables $\boldsymbol{S}'$ and $\boldsymbol{y}'$ that represent the column-wise concatenation of the real and imaginary parts of $\boldsymbol{S}$ and $\boldsymbol{y}$ respectively, such that $\boldsymbol{S}' \in \mathbb{R}^{2N\times M}$ and $\boldsymbol{y}' \in \mathbb{R}^{2N}$. The new subproblem is as follows:

$$\min_{\hat{\boldsymbol{a}}} ||\boldsymbol{S}'\hat{\boldsymbol{a}} - \boldsymbol{y}'||_2 \quad \text{subject to} \quad \hat{\boldsymbol{a}} \geq \boldsymbol{0} \tag{9}$$

and is solved using the Lawson-Hanson non-negative least-squares algorithm (NNLS) (21) to ensure non-negativity. This is a similar approach to that used in AQSES (11, 22).

Further prior knowledge can be incorporated into the model by applying soft constraints to $\hat{\boldsymbol{a}}$ using the weighting method, originally proposed by Lawson and Hanson (21). This method has been shown to offer advantages over hard-constraints when applied to self-modelling curve resolution (SMCR) (23) and can be conveniently integrated into the least-squares problem. To the best of the authors knowledge, this is the first time that the weighting method has been applied to the analysis of NMR data.

To demonstrate how the weighting method can be used to encourage a particular amplitude ratio between two elements of the basis set, let column $u, v$ be the indices of the columns corresponding to two basis vectors for which the desired ratio is $r_u/r_v$. For example, for NAA and NAAG we might put $r_u = 1$ and $r_v = 0.15$. We augment the least-squares problem as follows:

$$\begin{bmatrix} \boldsymbol{S}'_1 & \boldsymbol{S}'_2 & \dots & \boldsymbol{S}'_u & \boldsymbol{S}'_v & \dots & \boldsymbol{S}'_M \\ 0 & 0 & \dots & \lambda\epsilon_u^{(n)} & 0 & \dots & 0 \\ 0 & 0 & \dots & 0 & \lambda\epsilon_v^{(n)} & \dots & 0 \end{bmatrix} \hat{\boldsymbol{a}} \approx \begin{bmatrix} \boldsymbol{y}' \\ \frac{r_u(a_u^{(n-1)} + a_v^{(n-1)})}{r_u + r_v}\lambda\epsilon_u^{(n)} \\ \frac{r_v(a_u^{(n-1)} + a_v^{(n-1)})}{r_u + r_v}\lambda\epsilon_v^{(n)} \end{bmatrix} \tag{10}$$

where $\epsilon_i = ||\boldsymbol{S}_i||_1$ representing the $l_1$ norm of the $i$-th column of $\boldsymbol{S}$, the value of $\lambda$ determines the strength of the constraint and the superscript $(n-1)$ or $(n)$ refers to the value of the variable at the previous or current iterations respectively. Denoting the augmented left and right hand sides of equation (10) as $\boldsymbol{S}'^{aug}$ and $\boldsymbol{y}'^{aug}$ respectively, we seek to solve the problem:

$$\min_{\hat{\boldsymbol{a}}} ||\boldsymbol{S}'^{aug}\hat{\boldsymbol{a}} - \boldsymbol{y}'^{aug}||_2 \quad \text{subject to} \quad \hat{\boldsymbol{a}} \geq \boldsymbol{0} \tag{11}$$

using NNLS as described previously.

Separation between lipid and macromolecule signals is difficult at low field strengths due to interference, and many broad signals are often required to produce an accurate model. The combination of high signal overlap and over-parameterisation result in a fitting problem that is poorly defined. Whilst some independence between lipid and macromolecular component amplitudes is required, certain amplitude combinations are very unlikely. For instance, the ratio between lipid resonances at 0.9ppm and 1.3ppm is unlikely to vary greatly due to their known structure. Soft constraints can be used to improve fitting stability for these signals by encouraging a particular ratio between them. Table 2 lists the soft ratio constraints used to be consistent with LCModel$^{\text{TM}}$and a $\lambda$ value of 0.05 was found to provide a weak level of bias and speed up the fitting convergence in

some cases.

An additional challenge in estimating lipid and macromolecular signals is due to their rapid decay in the time-domain, causing their estimates to become highly unstable once $n_s$ is too great. This can lead to incorrectly high amplitudes for broad signals resulting in irregular baselines and poor residuals in the frequency domain. To reduce this problem, soft constraints are added to introduce a bias for solutions where the signal amplitudes are small, achieved by augmenting $\boldsymbol{y}'$ with a zero, and all columns of $\boldsymbol{S}$ with $\zeta\epsilon_i$ where $\zeta$ is the strength of the bias. In the normal case this bias should be too small to have an influence on the estimates, however when the data is noisy or when $n_s$ is too great, the bias has a stabilising effect on fitting.

Figure 1 demonstrates how the bias can stabilise the fitting, preventing broad signals such as lipids and macromolecules from being overestimated. From testing with a number of experimental spectra (see section Method Validation) a $\zeta$ value of 0.05 was found to be good compromise between stabilising the results and introducing unwanted bias.

The non-linearly entering parameters in equation (6) are found using an implementation of the Levenberg-Marquardt optimisation algorithm that allows hard constraints to be specified (24). The following hard constraints were applied to the non-linearly entering parameters: $-2\pi \leq \Delta\phi_0 \leq 2\pi$; $-\pi/4 \leq \Delta\phi_1 \leq \pi/4$; $0\text{Hz}^2 \leq \beta \leq 5000\text{Hz}^2$; $-0.03\text{ppm} \leq \Delta\omega_i \leq 0.03\text{ppm}$; $0\text{Hz} \leq \Delta\alpha_i \leq 10\text{Hz}$. The maximum permitted frequency shift and damping was increased to $-0.05\text{ppm} \leq \Delta\omega_i \leq 0.05\text{ppm}$ and $0\text{Hz} \leq \Delta\alpha_i \leq 50\text{Hz}$ for lipid and macromolecule signals as they have a higher level of variability than metabolites.

When solving the problem of equation (6) a considerable reduction in the time required for convergence can be achieved if an analytic expression for the Jacobian is available; the alternative is a computationally expensive numerically approximated version. We have derived an accurate analytic approximation to the Jacobian, which is both faster and more accurate than the numerical equivalent [1].

### 2.1.7 Use of Water Reference Signal for Absolute Concentrations

It is often desirable for the amplitudes of signals estimated to be expressed in absolute units. One popular method for absolute quantitation, uses the fact that the concentration of water $W_{conc}$ is often known for a particular tissue type. Concentrations of the signals in mM units can therefore be obtained by scaling the fitted signal amplitudes by the amplitude of the unsuppressed water resonance, usually obtained from an additional experiment where the water suppression method is omitted from the pulse sequence. A detailed description of the steps required for the measurement

[1] Details available by request.

of water content are described by Ernst et al. (25). An additional scaling factor $W_{att}$ is required that takes account of any additional attenuation of the unsuppressed water signal compared to the water suppressed signal. This is typically due to transverse relaxation differences between the metabolite and water signals with a typical $T_2$ of water reported as 80ms by Ernst et al (25). At an echo time of 30ms the expected attenuation can be calculated as $W_{att} = \exp(-TE/T_2) \approx 0.7$ and this is the default value used in TARQUIN.

The TARQUIN algorithm automatically measures the amplitude of the unsuppressed water signal $a_{water}$ when an appropriate data file is specified by the user, and scales the signal amplitudes $\hat{\boldsymbol{a}}$ appropriately based on the values of $W_{conc}$ and $W_{att}$. Water is the dominant signal when water suppression is omitted, therefore its amplitude can be simply estimated in the time domain by performing a least squares exponential fit of the FID. Since the exact frequency and phase of this signal is unknown, the fitting problem can be simplified by fitting the magnitude of the complex signal $|\boldsymbol{y}_W[n]|$ that is assumed to have the following form:

$$|\boldsymbol{y}_W[n]| = a_w \exp(Bn\Delta t) \tag{12}$$

where $a_w$ is the amplitude of the water signal and $B$ is an exponential decay constant. The amplitude $a_w$ can be found by minimising the following function using standard methods:

$$\sum_{n=n_{ws}}^{n_{we}} |\boldsymbol{y}_W[n]|(\ln|\boldsymbol{y}_W[n]| - \ln a_w - Bn\Delta t)^2 \tag{13}$$

where $n_{ws}$ and $n_{we}$ specify a segment of the FID to be analysed. Logarithms are used to transform the problem into one that can be solved using linear methods and the additional factor ($|\boldsymbol{y}_W[n]|$) is applied to weight the points equally. For best results $n_{ws}$ and $n_{we}$ should be chosen to skip the distorted region of the FID, and fit only a small section to ensure the assumption of exponential decay is valid. Visual inspection of a number of FIDs revealed that distortions at the beginning of the data did not exceed beyond the 9th data point therefore a value of 10 was chosen for $n_{ws}$. A value of 50 was chosen for $n_{we}$ so that only a relatively short section of the FID was fitted since the differences between a Lorentzian and Gaussian decay are less pronounced over a shorter data range.

A numerical simulation was performed to test the validity of the simplistic model of the water signal. To test the influence of a non Lorentzian lineshape on water amplitude estimation, Lorentzian and Gaussian signals were simulated, each with a FWHM of 4.8Hz. Comparing the amplitude estimations of simulated Lorentzian and Gaussian water signals revealed that the am-

plitude of the Gaussian signal was overestimated by 1.4%, which is small enough for the majority of purposes. The amplitude estimation of the Lorentzian signal was perfect as expected. It should also be noted that visual inspection of the fits to real water signals revealed that the Lorentzian approximation is typically very good, so errors would be expected to be much smaller than 1.4%.

An additional source of potential bias may arise from non-water signals having a significant contribution to the data. Since lipids are known to be highly elevated in some tumours, the water unsuppressed spectrum from patient with Grade 4 Glioblastoma multiforme was inspected to assess their contribution. No clear lipid signals were observed despite their high presence in the water suppressed spectrum, confirming that the water signal is several orders of magnitude higher than any other signals that could confound amplitude estimation. Whilst the water signal model presented is valid for brain tissue, other tissues containing a higher lipid:water ratio may require the non-water signals to be removed prior to amplitude estimate.

### 2.1.8 Post Processing

The final steps in the TARQUIN algorithm are purely for visualising the results and have no influence on the amplitude estimates. In the optimisation part of the algorithm, the $\Delta\phi_0$ and $\Delta\phi_1$ parameters are applied to the basis signals and therefore $\hat{\boldsymbol{y}}$. To assist the visual interpretation of the fit, the additive inverse of these parameters are applied to $\boldsymbol{y}$ rather than the basis set, causing the basis set to always be correctly in-phase.

The signals $\boldsymbol{y}$ and $\hat{\boldsymbol{y}}$ are zero-filled to 4096 points prior to Fourier transformation to increase their digital resolution. The residual $R$ is formed as follows:

$$R = \boldsymbol{y} - \hat{\boldsymbol{y}} \tag{14}$$

since the residual is expected to consist primarily of noise and smooth baseline imperfections, the baseline $B$ can be extracted from $R$ by applying an appropriate smoothing filter. Whilst the choice of filter does not influence the quantification, an appropriate response can reveal signals that are missing from the basis set and identify broad artefacts present in the spectrum. Allowing too much flexibility in the baseline will result in the noise being modelled (overfitting) and obscure problems associated with an incomplete basis. Not having enough flexibility will result in broad signals being present in the residual and this can make assessment of fit quality more difficult. A range of filter widths were tested on our data and a convolution of $B$ with a Gaussian window function around 100 data points in width gave appropriate looking baselines.

A linear extrapolation was finally applied to the baseline at the edges of the spectrum as the

convolution procedure cannot be applied here. Details of the convolution method can be found in the post acquisition solvent suppression paper by Marion et al. (26).

### 2.1.9 Implementation Details

An open-source implementation of our algorithm is available for both Microsoft Windows and GNU/Linux. Written in C++ and GPL-licenced, it includes a command-line interface, suitable for batch processing, and a GUI interface, suitable for interactive use. At the time of writing, data import functionality is available for the following SVS data formats: GE P-files, Siemens RDA, Philips SDAT/SPAR, Bruker fid files and Varian fid files.

## 2.2 Method Validation

### 2.2.1 Healthy Volunteer Data

Since numerous reports have been published on $^1$H MRS performed on healthy volunteers, this data type is ideal for comparing and validating fitting methods. Six healthy adult males in the age range of 21 to 54 years were studied. Scanning was performed on a 3T Philips Achieva scanner using an 8-element sense head coil. Sagittal and axial $T_1$-weighted localizer images were acquired and used for voxel placement. A 20mm x 20mm x 20mm voxel was placed in the right parieto-occipital white matter of each volunteer as shown in Figure 2. The PRESS sequence was chosen for $^1$H MRS with an echo time of 35ms, spectral width of 2000Hz and 1024 complex points were acquired. 128 scans with a repetition time of 2 seconds were acquired for the water suppressed data and 16 scans with a repetition time of 5 seconds were acquired for the water unsuppressed data. Each spectrum was analysed with the TARQUIN algorithm as presented and LCModel$^{TM}$ (version 6.2-1L).

A recent study by Baker et al. (27) reports the $^1$H MRS metabolite concentrations from various locations within the healthy adult brain, as determined by LCModel$^{TM}$. This study was chosen as the primary comparator to our results as it was performed at 3T using a short-echo time PRESS sequence. In the paper, correction factors are applied to the metabolite concentrations to account for metabolite $T_1$ and $T_2$ relaxation effects. To ensure concentrations are directly comparable, the same correction factors were applied to our results. To obtain metabolite quantities in molar units, the NMR-visible molar concentration of water in tissue was assumed to be 35.88 moles per litre, consistent with Baker et al.

To asses the agreement between LCModel$^{TM}$ and TARQUIN, a Bland Altman (28) analysis was performed on each metabolite quantity reported by Baker et al. The average of the upper

and lower-limits of agreement, which represent the 95% confidence intervals of agreement, were calculated for each metabolite to estimate the agreement between the two methods.

### 2.2.2 Monte-Carlo Simulation

Whilst $^{1}$H MRS performed on healthy volunteers is convenient to obtain, is has the disadvantage that the true metabolite concentrations are unknown, making it inappropriate for measuring accuracy. Alternatively, phantoms containing solutions of metabolites at known concentration can be used to measure accuracy, however results can be trivial as this method does not model important baseline effects caused by macromolecules. In addition, metabolites in solution can chemically degrade over time, for example NAA will degrade into Asp and Ace, making results difficult to interpret. The method of Monte-Carlo simulation makes a good alternative to phantom studies since true metabolite quantities are known to numerical accuracy. In addition, other spectral properties such as noise, lineshape and baseline effects can be easily modelled and controlled.

To obtain realistic simulated spectra, signal components were simulated at the same concentrations obtained from the average LCModel$^{TM}$ results obtained from the healthy volunteer data. Additional Gaussian line broadening of 4Hz was applied to the metabolite and lipid/macromolecular components of the signal to model the effects of imperfect shimming and in-vivo T2 relaxation. The following additional modifications were made to the simulated FID to model common artefacts typically observed in in-vivo MRS:

- Complex Gaussian noise with a standard deviation of 1 was added, which corresponded to an SNR of 21 as determined by LCModel$^{TM}$.
- Complex Gaussian noise with a standard deviation of 50 was added to the first 4 data points to mimic baseline artefacts.
- A simulated residual water peak with a concentration of 500mM and a phase shift of 25° was added.

An additional water unsuppressed signal was generated to investigate any systematic errors that may be introduced by the estimation of the water amplitude. 100 water suppressed spectra were synthesised with different noise values while baseline noise and all other signals were kept constant. Each spectrum was analysed with both TARQUIN and LCModel$^{TM}$ (version 6.2-1L), and the average and standard deviation of each metabolite concentration was calculated.

### 2.2.3 Clinical Data

A further disadvantage of using healthy volunteer spectra to validate fitting is that often it is pathological brain tissue which is of interest. This data type is generally of poorer quality and can often contain high levels of lipids and other molecules not seen in healthy brain tissue. It is therefore important to test any new method on a large set of clinical data before it can be regarded as robust to noisy, abnormal, artefactual and poorly shimmed spectra.

The cohort consisted of eligible patients undergoing MR imaging at Birmingham Children's Hospital as part of their clinical investigations. Approval for the study was obtained from the research ethics committee and informed consent was taken from parents/guardians. MRI and MRS were carried out on a 1.5T Siemens Symphony Magnetom, with a single channel head coil, and a 1.5T GE Signa Excite scanner equipped with an 8 channel head coil.

Point resolved single voxel spectroscopy (PRESS) was performed on the suspected area of pathology (29) with a short echo time (TE=30ms) and a repetition time of 1500ms. In some cases an additional scan was performed with a long echo time (TE=135ms). Cubic voxels of either 20mm or 15mm length were used depending on the size of the lesion. Water suppressed data was acquired with 128 repetitions from the larger voxels and 256 repetitions from the smaller ones. A corresponding water unsuppressed spectrum was also acquired with 4 scans for use as a concentration reference.

The quality of the fitting results were assessed in two ways. Firstly, a measure of the fit quality ($Q$) was determined for each spectrum analysed. $Q$ was defined as the standard deviation of the frequency domain residual between 0.2 and 4.0ppm divided by the standard deviation of the spectral noise. This definition, similar to that of Slotboom et al (30), has the attribute that $Q$ will be: less than unity where overfitting has occurred; equal to unity where the fit is perfect; greater than unity when the signal has not been completely modelled. $Q$ cannot be used to identify baseline problems, and has the counter intuitive property that adding random noise to a fit will improve the fit quality (unless $Q = 0$). However, it is useful for assessing fit quality for large numbers of spectra, where manual inspection is not feasible.

The second method for measuring fit quality was to randomly select 100 short echo time spectra analysed. Each fit was visually inspected to identify any fitting problems which may not be possible to detect using $Q$.

# 3 Results

## 3.1 Healthy Volunteer Data

Figure 3 shows fits to a typical spectrum of para-occipital white matter using a short echo time sequence at 3T. The influence of the $n_s$ parameter is illustrated in parts a) and b), where a higher value of $n_s$ gives a baseline that is closer to the acquired data. This demonstrates how the preference for lower signal amplitudes, given by the weighting method, influences the baseline as more points are truncated in the time-domain.

An LCModel$^{TM}$ analysis of the same spectrum (Figure 3c)) shows a greater similarity to the TARQUIN analysis with $n_s$=20 particularly in the section of baseline between 3.5 and 4ppm. The main difference between the LCModel$^{TM}$ and TARQUIN analyses is in the fitting of the macromolecule peak at 0.9ppm, where LCModel$^{TM}$ shows an overestimation of this signal resulting in a dip in the baseline. Comparing the residuals in this region shows near identical results for each fit, whereas the baseline is much smoother in TARQUIN because of the soft constraints placed on signal amplitudes. Another minor difference present between parts a) and c) is in the residual of the TNAA peak where LCModel$^{TM}$ shows a smaller residual, probably on account of its more flexible line-shape modelling. Comparing fits from the other 5 spectra revealed similar features, with TARQUIN generally producing a more realistic baseline than LCModel$^{TM}$ using the default options for both algorithms. It was also noted that the LCModel$^{TM}$ residual was generally smaller, particularly around strong singlets. However, both differences were minor and did not have a significant effect on the metabolite estimates described subsequently.

The corresponding mean metabolite concentrations for the six volunteers are listed in Table 3 and the values determined by Baker et al (27) are provided for comparison. The best overall agreement in metabolite values between TARQUIN and LCModel$^{TM}$ was found using an $n_s$ value of around 20, which corresponded to a truncation of 10ms. Truncating fewer points resulted in a general increase in the metabolite concentration estimates, since the broader signal components present in the initial data points were modelled using the basis set. In particular, Glx and m-Ins showed the greatest dependence on $n_s$ due to their interference with broad signals around 2.2 and 3.55ppm respectively.

A Bland Altman analysis of the agreement between LCModel$^{TM}$ and TARQUIN with $n_s$=20 showed that 95% of measurements of Cr, TNAA, TCho and Ins agreed with an error smaller than approximately 20%. Glx agreed with an error smaller than approximately 40%, an increase likely due to an interference with macromolecular signals. Overall, the agreement in metabolite concentrations between TARQUIN, LCModel$^{TM}$ and published values was acceptable for most

purposes.

## 3.2 Monte-Carlo Simulation

An example simulated spectrum is shown in Figure 4 that is comparable to the experimental spectrum shown in Figure 3, with the exception of the macromolecular peak at 0.9ppm. This signal shows a greater spectral contribution since LCModel$^{TM}$ had a tendency to overestimate this signal.

The results from the Monte-Carlo simulation are shown in Figure 5. Some minor biases are present for low concentration and overlapping metabolites, for example LCModel$^{TM}$ overestimates Asp, whereas TARQUIN underestimates GPC due to its overlap with PC. In general, both methods give good estimates on average with little to separate the two in terms of accuracy. Comparing the theoretical errors with the observed errors shows a good agreement, implying that the main source of inaccuracy can be attributed to noise.

## 3.3 Clinical Data

1399 short and 557 long echo time spectra were analysed using TARQUIN and a summary of their fit quality is given in Table 4. No spectra had a $Q$ value of less than one, therefore we can be confident that the level of freedom used to model the baseline was not high enough to result in overfitting. The majority (77%) of spectra analysed had a fit quality number between one and two, and the median value of $Q$ was found to lie between 1.15 and 1.2. To illustrate the appearance of a well and poorly fitted spectrum two typical fits are shown in Figure 6. It is clear from part b) of Figure 6 that the high value of $Q$ is mainly due to the artefacts present between 0.2 and 2.0ppm and this was a common feature seen in the poorly fitted spectra.

A subset of 100 short echo time spectra analysed were also visually inspected. The vast majority of these spectra were fitted well, ie comparable to the fit shown in Figure 6a). One spectrum was fitted poorly due to a residual water signal at 3.7ppm, however an increase in the frequency range of the HSVD water removal step to 60Hz corrected this problem.

Figure 7 shows TARQUIN fits to three example childhood brain tumour spectra acquired at 1.5T. Part a) shows noisy data with small baseline distortions that can occur when out of volume signals are present, b) shows a spectrum with very little NAA, which can cause problems for finding the correct ppm reference value and c) shows a spectrum containing high levels of lipids, often seen in necrotic tissue. Small residuals and smooth baselines are shown for all three spectra that exhibit features, typically seen in pathology, that can hamper analysis.

# 4 Discussion

In this report, a new time-domain fitting algorithm is proposed that uses a novel regularised non-negative least squares projection method to estimate signal amplitudes. Whilst the core fitting algorithm is general enough for various MRS data types, we have chosen to focus on the automated analysis of short-echo $^1$H MRS data as it is one of the most popular clinical applications of MRS. The QUEST algorithm has been shown to effective for the analysis of short-echo $^1$H MRS data (31), however the current implementation (32) has a greater focus on the user to supply data processing options, making it better suited to a research environment where a greater level of flexibility is preferred. For large clinical data sets, we have found the automation and simplicity of LCModel$^{TM}$ to be an important feature and for this reason it has been chosen as a comparator.

An important factor in automating analysis is ensuring that the default fitting parameters are suitable for the data. In this work, an appropriate set of default parameter values have been tested and established using a set of short-echo $^1$H MRS spectra acquired clinically. With these starting values, the method can be used with minimal user interaction making it suitable for clinical applications.

We have found that TARQUIN produces fully automatic results comparable to LCModel$^{TM}$ with the advantage that baselines are often smoother. One area where LCModel$^{TM}$ may be advantageous over TARQUIN is where the lineshape is heavily distorted or asymmetric. In these cases, LCModel$^{TM}$ found a smaller residual on account of the extra freedom allowed in the fitting model. One possible improvement in this area would be to perform the QUALITY (33) lineshape correction algorithm in the preprocessing phase of TARQUIN. Overall, however we have found significant distortions of this type to be rare. Whilst analyses can be performed automatically, this does not guarantee good results for heavily distorted data, therefore inspection of results by an experienced spectroscopist or a suitable algorithm (34, 35) is always recommended before interpreting concentration estimates.

It has been noted that the separation of metabolite signals from lipid, macromolecules and baseline is important for accurate concentration estimates (10). The results shown in Table 3 show a dependence on the number of initial points removed, supporting this hypothesis, and demonstrate that the glutamate and glutamine resonances are particularly vulnerable to errors of this type. The two main algorithmic strategies taken to model lipid and macromolecular signals are to incorporate them into the baseline (default strategy of QUEST and AQSES), or include simulated signals in the basis set to fit these components directly (default strategy of LCModel$^{TM}$ and TARQUIN) (36). Adding broad lipid and macromolecular components to the basis set has the disadvantage of

increasing the risk of over-parametrisation, however since high lipids are known to be an important marker of malignancy, necrosis and cell death (37), determining their concentration can be clinically useful (38, 39).

An alternative to modelling lipid and macromolecular signals as part of fitting, is to use an experimental method to acquire a "metabolite-nulled" spectrum (40) and incorporate it into the analysis. However, a detailed study by Gottschalk et al. (41) demonstrated that the advantages over initial point truncation were minor, since perfect metabolite-nulling was not possible using a inversion recovery based sequence. Whilst this method may be preferred where the study of macromolecules is the primary goal, the additional scan time required, combined with the relatively minor improvement in metabolite estimation, make the method difficult to justify in a clinical setting.

Finally, whilst this work has focused on the application of the fitting routine to short-echo time *in-vivo* $^{1}$H SVS data from the brain, the core fitting algorithm is generic, and could be easily applied to other MRS data types such as chemical shift imaging or $^{31}$P MRS.

# 5 Conclusions

In this study, TARQUIN has been shown to be accurate, robust to poor quality data and in agreement with the popular frequency domain fitting program LCModel$^{TM}$ for the analysis of short echo time *in-vivo* $^{1}$H MRS data. An implementation of the algorithm, which includes the HSVD method for water removal and basis-set simulation functionality, is provided free of charge from http://tarquin.sourceforge.net.

# 6 Acknowledgements

This work was funded by the Medical Research Council, EU FP6 projects eTUMOUR and Health Agents, Cancer Research UK, EPSRC and the Department of Health. We would like to thank the Birmingham Children's Hospital Radiology Department, in particular Lesley MacPherson, Shaheen Lateef and Rachel Grazier for performing the spectroscopy and organising the raw data. We would also like to thank Yun Sun and Nigel Davies for organising the raw data. We would like to thank M.I.A. Lourakis for his free implementation of the Levenberg-Marquardt optimisation algorithm (levmar) used in TARQUIN which can be obtained from http://www.ics.forth.gr/∼lourakis/levmar. Finally, we would like to thank Jack van Asten for helpfully suggesting the automated phasing method described in the methods section.

# References


[1] Poullet JB, Sima DM, Van Huffel S. MRS signal quantitation: a review of time- and frequency-domain methods. J Magn Reson 2008;195:134–144.

[2] Barkhuijsen H, de Beer R, Bovee WMMJ, van Ormondt D. Retrieval of frequencies, amplitudes, damping factors, and phases from time-domain signals using a linear least-squares procedure. J Magn Reson 1985;61:465–481.

[3] Barkhuijsen H, de Beer R, van Ormondt D. Improved algorithm for noniterative and time-domain model fitting to exponentially damped magnetic resonance signals. J Magn Reson 1987;73:553–557.

[4] Millhauser GL, Carter AA, Schneider DJ, Freed JH, Oswald RE. Rapid singular value decomposition for time-domain analysis of magnetic resonance signals by use of the lanczos algorithm. J Magn Reson 1989;82:150–155.

[5] Vanhamme L, van den Boogaart A, Van Huffel S. Improved method for accurate and efficient quantification of MRS data with use of prior knowledge. J Magn Reson 1997;129:35–43.

[6] van der Veen JW, de Beer R, Luyten PR, van Ormondt D. Accurate quantification of in vivo 31P NMR signals using the variable projection method and prior knowledge. Magn Reson Med 1988;6:92–98.

[7] Mekle R, Mlynárik V, Gambarota G, Hergt M, Krueger G, Gruetter R. MR spectroscopy of the human brain with enhanced signal intensity at ultrashort echo times on a clinical platform at 3T and 7T. Magn Reson Med 2009;61:1279–1285.

[8] Kanowski M, Kaufmann J, Braun J, Bernarding J, Tempelmann C. Quantitation of simulated short echo time 1H human brain spectra by LCModel and AMARES. Magn Reson Med 2004; 51:904–912.

[9] Provencher SW. Estimation of metabolite concentrations from localized in vivo proton NMR spectra. Magn Reson Med 1993;30:672–679.

[10] Ratiney H, Sdika M, Coenradie Y, Cavassila S, van Ormondt D, Graveron-Demilly D. Time-domain semi-parametric estimation based on a metabolite basis set. NMR Biomed 2005; 18:1–13.

[11] Poullet JB, Sima DM, Simonetti AW, De Neuter B, Vanhamme L, Lemmerling P, Van Huffel S. An automated quantitation of short echo time MRS spectra in an open source software environment: AQSES. NMR Biomed 2007;20:493–504.

[12] Reynolds G, Wilson M, Peet A, Arvanitis TN. An algorithm for the automated quantitation of metabolites in *in Vitro* NMR signals. Magn Reson Med 2006;56:1211–1219.

[13] Schulte RF, Boesiger P. ProFit: two-dimensional prior-knowledge fitting of J-resolved spectra. NMR Biomed 2006;19:255–263.

[14] Vanhamme L, Fierro RD, Van Huffel S, de Beer R. Fast removal of residual water in proton spectra. J Magn Reson 1998;132:197–203.

[15] Levitt MH. Spin Dynamics: Basics of Nuclear Magnetic Resonance. Wiley, 2001.

[16] Smith S, Levante T, Meier B, Ernst R. Computer simulations in magnetic resonance. an object-oriented programming approach. J Magn Reson 1994;106a:75–105.

[17] de Graaf R. in vivo NMR spectroscopy - principles and techniques. Wiley, 2007.

[18] Govindaraju V, Young K, Maudsley AA. Proton NMR chemical shifts and coupling constants for brain metabolites. NMR Biomed 2000;13:129–153.

[19] Wilson M, Davies NP, Sun Y, Natarajan K, Arvanitis TN, Kauppinen RA, Peet AC. A comparison between simulated and experimental basis sets for assessing short-echo time *in-vivo* 1H MRS data at 1.5T. NMR Biomed 2010;In Press.

[20] Marshall I, Higinbotham J, Bruce S, Freise A. Use of Voigt lineshape for quantification of *in vivo* $^{1}$H spectra. Magn Reson Med 1997;37:651–657.

[21] Lawson CL, Hanson RJ. Solving Least Squares Problems. SIAM, 1995.

[22] Sima DM, Van Huffel S. Separable nonlinear least squares fitting with linear bound constraints and its application in magnetic resonance spectroscopy data quantification. J Comput Appl Math 2007;203:264–278.

[23] Gemperline PJ, Cash E. Advantages of soft versus hard constraints in self-modeling curve resolution problems. alternating least squares with penalty functions. Anal Chem 2003;75:4236–4243.

[24] Kanzow C, Yamashita N, Fukushima M. Levenberg-Marquardt methods with strong local convergence properties for solving nonlinear equations with convex constraints. J Comput Appl Math 2004;172:375–397.

[25] Ernst T, Kreis R, Ross B. Absolute quantitation of water and metabolites in the human brain. 1. Compartments and water. J Magn Reson 1993;102:1–8.

[26] Marion D, Ikura M, Bax A. Improved solvent suppression in one-dimensional and two-dimensional NMR spectra by convolution of time-domain data. J Magn Reson 1989;84:425–430.

[27] Baker EH, Basso G, Barker PB, Smith MA, Bonekamp D, Horská A. Regional apparent metabolite concentrations in young adult brain measured by (1)H MR spectroscopy at 3 Tesla. J Magn Reson Imaging 2008;27:489–499.

[28] Bland JM, Altman DG. Statistical methods for assessing agreement between two methods of clinical measurement. Lancet 1986;1:307–310.

[29] Barkovitch AJ. Pediatric Neuroimaging. Lippincott Williams & Wilkins, 2005.

[30] Slotboom J, Nirkko A, Brekenfeld C, van Ormondt D. Reliability testing of in vivo magnetic resonance spectroscopy (MRS) signals and signal artifact reduction by order statistic filtering. Measurement Science and Technology 2009;20:104030.

[31] Malucelli E, Manners DN, Testa C, Tonon C, Lodi R, Barbiroli B, Iotti S. Pitfalls and advantages of different strategies for the absolute quantification of N-acetyl aspartate, creatine and choline in white and grey matter by 1H-MRS. NMR Biomed 2009;22:1003–1013.

[32] Naressi A, Couturier C, Devos JM, Janssen M, Mangeat C, de Beer R, Graveron-Demilly D. Java-based graphical user interface for the MRUI quantitation package. MAGMA 2001; 12:141–152.

[33] de Graaf AA, van Dijk JE, Bove WM. QUALITY: quantification improvement by converting lineshapes to the Lorentzian type. Magn Reson Med 1990;13:343–357.

[34] Kreis R. Issues of spectral quality in clinical 1H-magnetic resonance spectroscopy and a gallery of artifacts. NMR Biomed 2004;17:361–381.

[35] Wright AJ, Arús C, Wijnen JP, Moreno-Torres A, Griffiths JR, Celda B, Howe FA. Automated quality control protocol for MR spectra of brain tumors. Magn Reson Med 2008;59:1274–1281.

[36] Seeger U, Klose U, Mader I, Grodd W, Nagele T. Parameterized evaluation of macromolecules and lipids in proton MR spectroscopy of brain diseases. Magn Reson Med 2003;49:19–28.

[37] Hakumaki JM, Kauppinen RA. 1H NMR visible lipids in the life and death of cells. Trends Biochem Sci 2000;25:357–62.

[38] Preul MC, Caramanos Z, Collins DL, Villemure JG, Leblanc R, Olivier A, Pokrupa R, Arnold DL. Accurate, noninvasive diagnosis of human brain tumors by using proton magnetic resonance spectroscopy. Nat Med 1996;2:323–5.

[39] Astrakas LG, Zurakowski D, Tzika AA, Zarifi MK, Anthony DC, De Girolami U, Tarbell NJ, Black PM. Noninvasive magnetic resonance spectroscopic imaging biomarkers to predict the clinical grade of pediatric brain tumors. Clin Cancer Res 2004;10:8220–8228.

[40] Behar KL, Rothman DL, Spencer DD, Petroff OA. Analysis of macromolecule resonances in 1H NMR spectra of human brain. Magn Reson Med 1994;32:294–302.

[41] Gottschalk M, Lamalle L, Segebarth C. Short-TE localised 1H MRS of the human brain at 3T: quantification of the metabolite signals using two approaches to account for macromolecular signal contributions. NMR Biomed 2008;21:507–517.

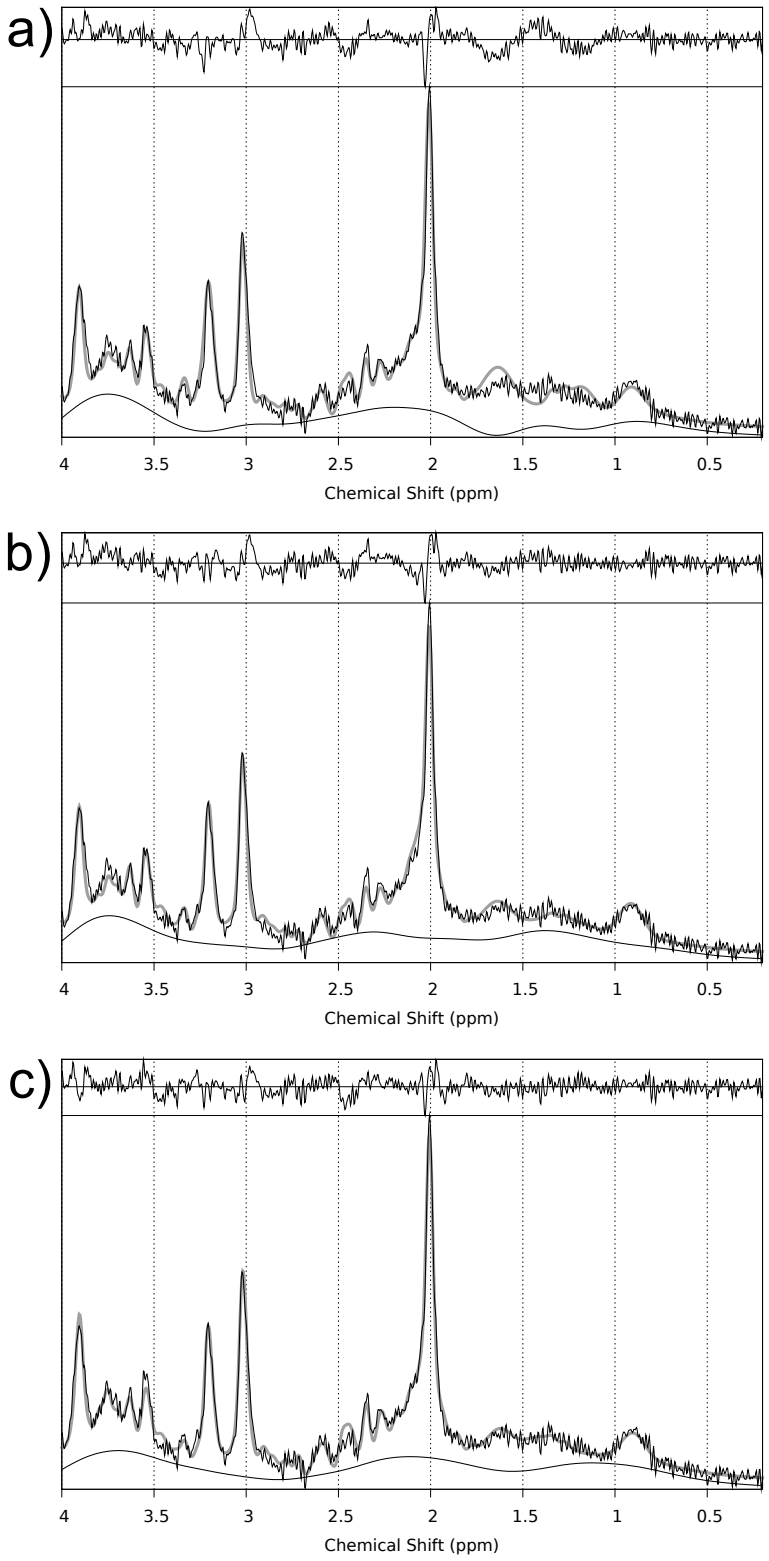


Figure 1: Example fits showing the influence of $n_e$ and $\lambda_s$ on the baseline and residual. The following values were used for each fit: a) $n_s = 45$ and $\lambda_s = 0$; b) $n_s = 45$ and $\lambda_s = 0.05$; and c) $n_s = 20$ and $\lambda_s = 0.05$. The acquired spectrum is plotted in black and the fit in grey. Below and above the acquired spectrum the baseline and residual are shown respectively.

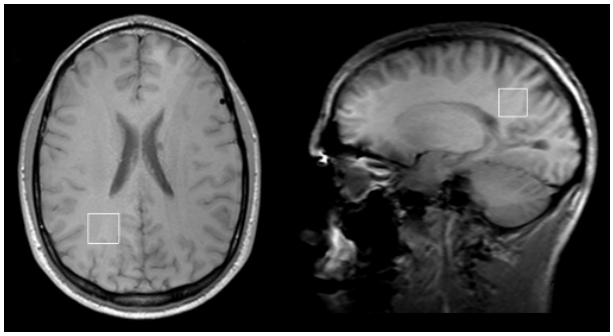

Figure 2: Para-occipital white matter voxel location for healthy volunteers.

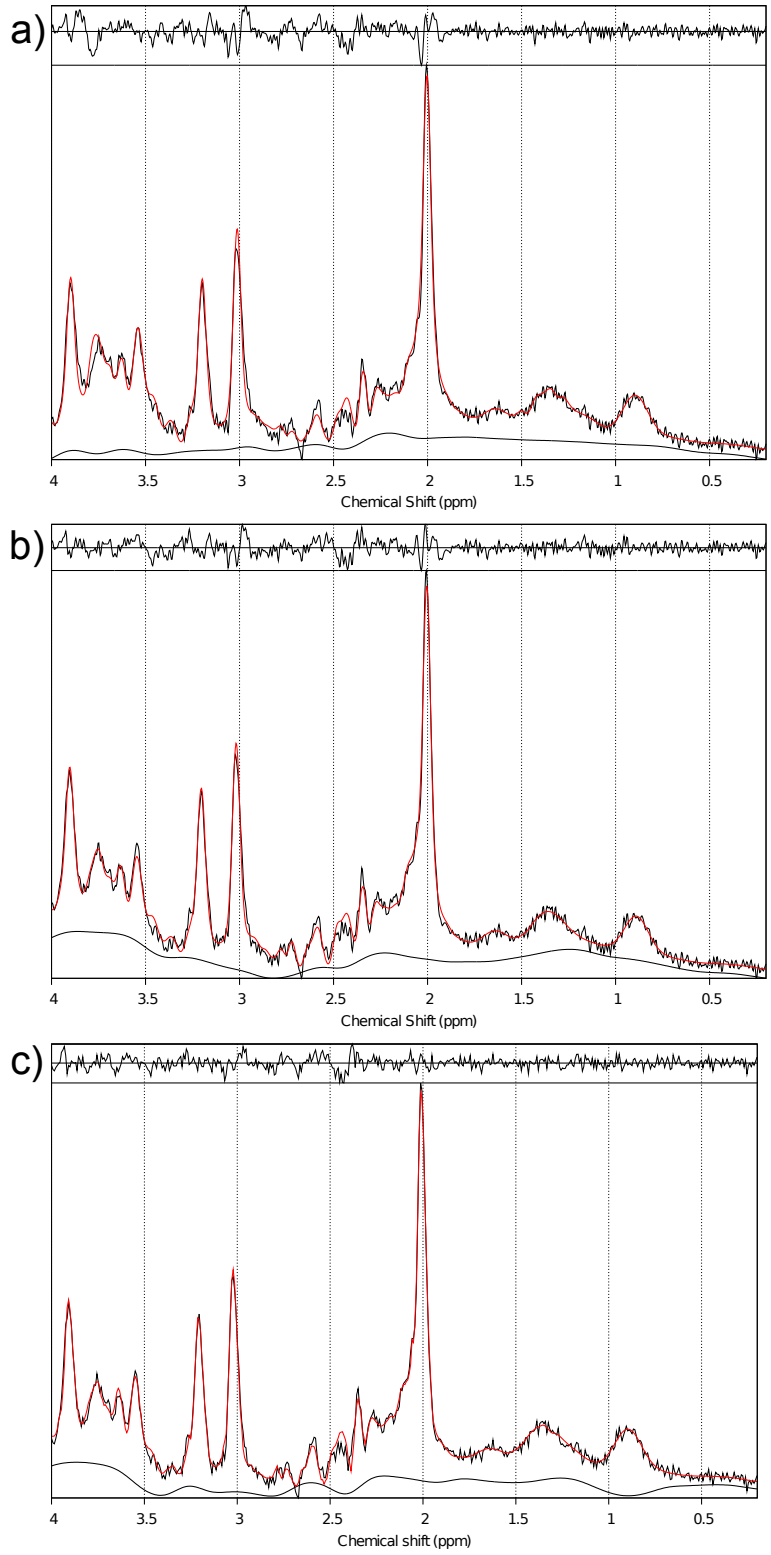


Figure 3: Healthy para-occipital white matter MRS fitting results from a) TARQUIN with $n_s$=5, b) TARQUIN with $n_s$=20 and c) LCModel$^{\mathrm{TM}}$. The acquired spectrum is plotted in black and the fit in red. Below and above the acquired spectrum the baseline and residual are shown respectively.

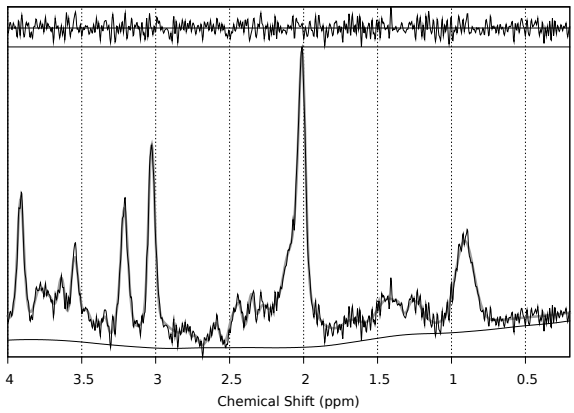


Figure 4: An example fit to a simulated spectrum. The acquired spectrum is plotted in black and the fit in grey. Below and above the acquired spectrum the baseline and residual are shown respectively.

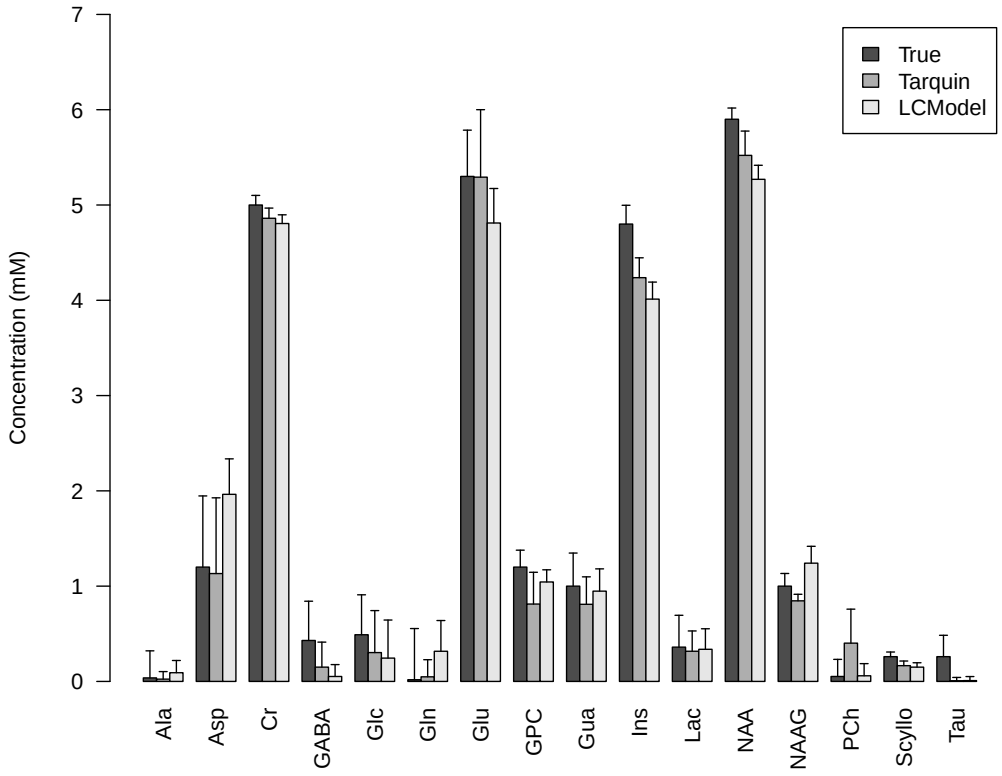


Figure 5: Monte-Carlo simulation results from TARQUIN and LCModel$^{TM}$ from spectra generated with a signal to noise ratio of 21. Error bars represent standard deviations determined from the Monte-Carlo simulation for TARQUIN and LCModel. Error bars shown for the true concentrations were calculated theoretically from the CRLBs.

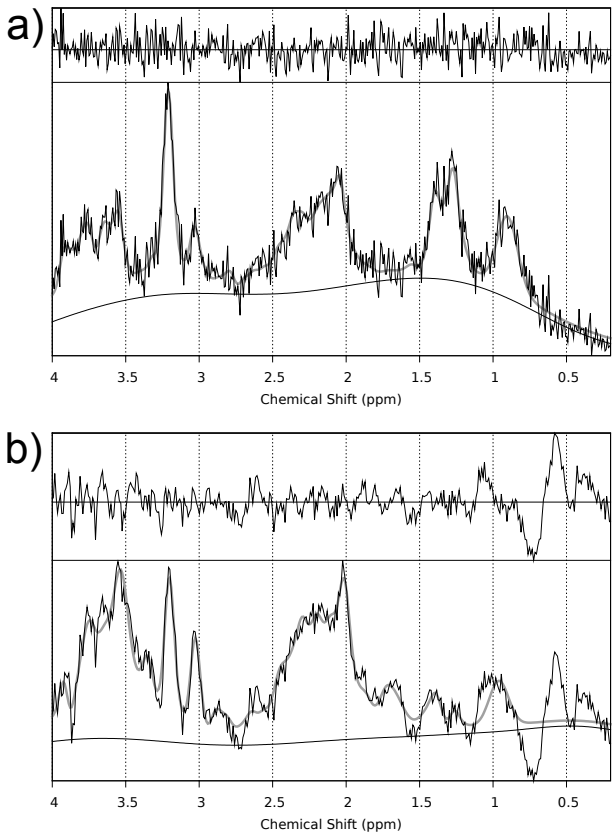


Figure 6: Two example fits to illustrate the appearance of a) well fitted data ($Q$=1.18) and b) poorly fitted data ($Q$=3.52). The acquired spectrum is plotted in black and the fit in grey. Below and above the acquired spectrum the baseline and residual are shown respectively.

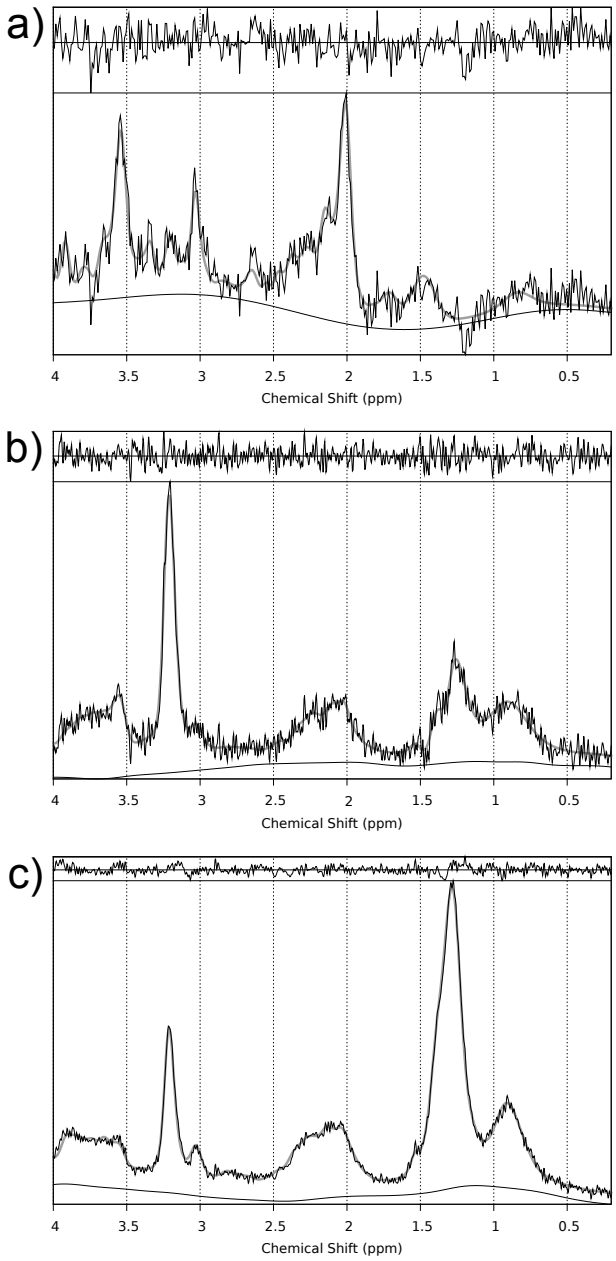


Figure 7: Example fits from a) noisy spectrum with a minor baseline distortion, b) spectrum with very low NAA and c) spectrum with strong lipid resonances. The acquired spectrum is plotted in black and the fit in grey. Below and above the acquired spectrum the baseline and residual are shown respectively.

| Signal | Freq (ppm) | FWHM (ppm) | Amplitude (au) |
|---|---|---|---|
| Lip13a | 1.28 | 0.15 | 2.0 |
| Lip13b | 1.28 | 0.89 | 2.0 |
| Lip09 | 0.89 | 0.14 | 3.0 |
| MM09 | 0.91 | 0.14 | 3.0 |
| Lip20 | 2.04 | 0.15 | 1.33 |
| Lip20 | 2.25 | 0.15 | 0.67 |
| Lip20 | 2.8 | 0.2 | 0.87 |
| MM20 | 2.08 | 0.15 | 1.33 |
| MM20 | 2.25 | 0.2 | 0.33 |
| MM20 | 1.95 | 0.15 | 0.33 |
| MM20 | 3.0 | 0.2 | 0.4 |
| MM12 | 1.21 | 0.15 | 2 |
| MM14 | 1.43 | 0.17 | 2 |
| MM17 | 1.67 | 0.15 | 2 |

Table 1: A table of parameters used to generate the lipid and macromolecule basis signals. Where signal names have been repeated, the listed components were summed to form a composite signal.

| Signals | Ratio |
|---|---|
| Lip09/Lip13 | 0.267 |
| Lip20/Lip13 | 0.15 |
| MM20/MM09 | 1.5 |
| MM12/MM09 | 0.3 |
| MM14/MM09 | 0.75 |
| MM17/MM09 | 0.375 |
| NAAG/NAA | 0.15 |

Table 2: A table of the soft constraints used in the fitting model.

| | TARQUIN $n_s$=5 | TARQUIN $n_s$=20 | LCModel | Published | Agreement |
|---|---|---|---|---|---|
| Cr | 8.25 (0.82) | 7.17 (0.80) | 6.69 (0.13) | 6.14 (0.92) | 1.52 |
| TNAA | 9.87 (0.72) | 8.90 (0.88) | 9.91 (0.68) | 10.97 (1.19) | 1.95 |
| TCho | 2.13 (0.17) | 1.91 (0.17) | 1.68 (0.11) | 1.60 (0.24) | 0.29 |
| Ins | 7.64 (1.12) | 4.30 (0.81) | 5.63 (0.57) | 3.30 (0.60) | 0.74 |
| Glx | 13.91 (3.89) | 6.98 (1.36) | 6.57 (1.16) | 6.48 (1.58) | 2.72 |

Table 3: A comparison of mean metabolite concentrations from healthy adult volunteers in the para-occipital white matter brain region between TARQUIN with $n_s$=5 and 20, LCModel$^{TM}$ and published values (27). Values are expressed in mM followed by the standard deviation in brackets where appropriate. All values are presented with an accuracy of two decimal places. The average limits of agreement, measured using the Bland Altman method, are also included to measure the agreement between LCModel and TARQUIN with $n_s$=20.

| Fit quality | % of spectra |
|---|---|
| $1 \geq Q$ | 0 |
| $2 \geq Q > 1$ | 77 |
| $3 \geq Q > 2$ | 15 |
| $Q > 3$ | 8 |

Table 4: A summary of the fit quality ($Q$) for the 1956 clinical spectra analysed.